Journal of Chromatography A, 1217 (2010) 7359–7371

Contents lists available at ScienceDirect

Journal of Chromatography A

journal homepage: www.elsevier.com/locate/chroma

Parametric uncertainties and influence of the dead volume representation in modelling simulated moving bed separation processes

V. Grosfils[a], R. Hanus[a], A. Vande Wouwer[b], M. Kinnaert[a,*]

[a] Service d'Automatique et d'Analyse des Systèmes, Université Libre de Bruxelles, CP 165/55, 50, Av. F. D. Roosevelt, B-1050 Brussels, Belgium
[b] Service d'Automatique, Faculté Polytechnique de Mons, Boulevard Dolez, 31, 7000 Mons, Belgium

ARTICLE INFO

Article history:
Received 1 June 2010
Received in revised form 5 September 2010
Accepted 8 September 2010
Available online 17 September 2010

Keywords:
Identification
Chromatography
Distributed parameter system
Dead volume

ABSTRACT

In this study, a systematic numerical procedure for identifying the model parameters of simulated moving bed (SMB) separation processes is developed. The parameters are first estimated by minimizing a weighted least-squares criterion using experimental data from batch experiments, e.g. the time evolution of the concentration of elution peaks. Then, a cross-validation is achieved using data from experiments in SMB operation. At this stage, the importance of a careful modelling of the dead volumes within the SMB process is highlighted. In addition, confidence intervals on the estimated parameters and on the predicted concentration profiles are evaluated.

1. Introduction

Conventional batch chromatography is relatively inefficient in terms of adsorbent and solvent consumption and significant benefits can be achieved by performing separation of high-added value products, such as enantiomers produced in the pharmaceutical industry, with a simulated moving bed (SMB) process. The SMB process allows a counter-current movement of the liquid and the solid to be achieved in order to increase the exchange capabilities between both phases. In practice, there is no real solid movement but a "simulated" counter-current. Indeed, the process is constituted by several fixed beds in series and the simulated solid movement is achieved by periodically switching the inlet and outlet valves by one column in the direction of the liquid flow. For further details about the process see [1].

This process has been used for large scale production in the petrochemical and sugar industry since the 1950's. However, the transfer of the SMB technology to the separation of fine chemicals is not immediate. Indeed, the conditions (characteristics of the phases, interactions, etc.) are very different. Moreover, product purity is also subject to tight constraints imposed by the pharmaceutical and food regulatory organisations. Furthermore, the optimal operating conditions, which, by definition, are achieved if the required purities are obtained with the highest possible productivity and the smallest possible solvent consumption, are not easy to determine. Most of the methods use a process model and are, thus, subject to modelling errors. Besides, the optimal conditions of the SMB operations are not robust to the changes of temperature, of the feed composition, or of the feed flow rate. Hence, most of the SMB units work on robust but suboptimal conditions. In this way, they satisfy to the specifications most of the time despite the disturbances. Indeed, in general, there is no closed loop control. To study these problems of selection of optimal operating conditions, process control and monitoring of the SMB process, a precise model of the plant is required. Indeed, such a model, able to reproduce with details the operation of the process, may generate fictitious data to tune and test the developed control and monitoring methods.

SMB models consist of mass balance equations in the liquid and in the solid phase of the components to separate. A first-principle SMB model usually includes the isotherm parameters, the column porosity, the diffusion and/or the mass transfer coefficients. Typically, all these parameters are determined from batch experiments, performed on analytical columns or on SMB columns.

In the literature, many comparisons have been performed between experimental concentration profiles and simulated profiles. In most of the presented results, discrepancies are observed between the experimental profiles and the simulated ones. Two critical points are mentioned. On the one hand, the parameters are often roughly estimated from few experiments [2–4] or modified heuristically to minimize the difference between both profiles like in [5,6]. On the other hand, the presence of the extra column dead volumes influences significantly the concentration profiles [3,7,8]. In the literature, the extra column dead volumes are taken into

* Corresponding author. Tel.: +32 2 650 22 87; fax: +32 2 650 26 77.
E-mail addresses: Alain.VandeWouwer@fpms.ac.be (A.V. Wouwer), michel.kinnaert@ulb.ac.be (M. Kinnaert).

0021-9673/$ – see front matter © 2010 Elsevier B.V. All rights reserved.
doi:10.1016/j.chroma.2010.09.030

account in the determination of the operating conditions by modifying the equations of the triangle theory in some papers [9–12] but the introduction of the dead volume in the SMB models is not often considered [7,9]. Hence, there is obviously a need for a systematic estimation procedure of the parameters of a SMB model and for an effective modelling of the extra column dead volumes.

The aim of this paper is to validate on experimental data the systematic approach to SMB processes model identification from batch experiments developed in [13]. The first step is the application of the parameter identification from batch experiments described in the reference. The second step is the cross-validation with SMB experiments so as to assess whether the parameters identified from batch experiments may be used in a SMB model. This part of the work requires the development of an extra column dead volume model.

The method for parameter identification [13] is based on the definition of a cost function, characterizing the difference between measured and simulated elution peaks, and its minimization using an appropriate numerical method. The procedure has been developed after a systematic study of parameter identifiability. Thanks to a sensitivity analysis, the number of elution peaks and the associated feed concentration needed to identify the parameters with good accuracy have been determined. Moreover, from a systematic comparison of the identifiability of the parameters of the kinetic, equilibrium dispersive and LDF models, together with the evaluation of the computational load associated to such models, it has resulted that a kinetic model yields an appropriate compromise between these criteria. Hence, the identification procedure consists of the simultaneous identification of the isotherm parameters and the mass transfer coefficients of a kinetic model from two elution peaks, one at analytic concentration and a second one at the highest possible concentration given the solubility limit. Because of the presence of local minima, a multi-start optimization procedure is advisable. It consists in performing several identifications from different initial values of the parameters. Besides, confidence intervals for the estimated parameters and of the simulation errors are computed.

The cross-validation with SMB experiments is performed on a preparative SMB unit (CSEP C912, Knauer, Berlin, Germany). In this installation, contrary to usual configurations where the inlet and outlet ports are switched, a multifunctional valve allows the rotation of the columns at each switching time. As pumps and detectors are introduced between the columns of this SMB process, it turns out that the extra-column dead volumes cannot be neglected. In this study, the model developed in [9] is adapted to this kind of SMB.

The text is organised as follows. The presentation of the considered SMB process is given in Section 2. Section 3 is devoted to the parameter estimation from batch experiments. SMB modelling is discussed in Section 4 and the cross-validation on SMB experiments is performed in Section 5.

2. System description

Fig. 1 shows the equivalent counter-current representation of a SMB process. The system is subdivided into 4 different sections delimited by several material flow outlets and inlets. The two inlets are the input of the mixture to be separated and the input of a desorbing solvent. The system also has two withdrawal ports, one for the raffinate which is constituted mostly of the less adsorbable component (component A) and another for the extract which mostly consists of the more retained component (component B). The movement of the liquid and solid phases, as well as the adsorption-desorption phenomena taking place in each section are depicted in Fig. 1.

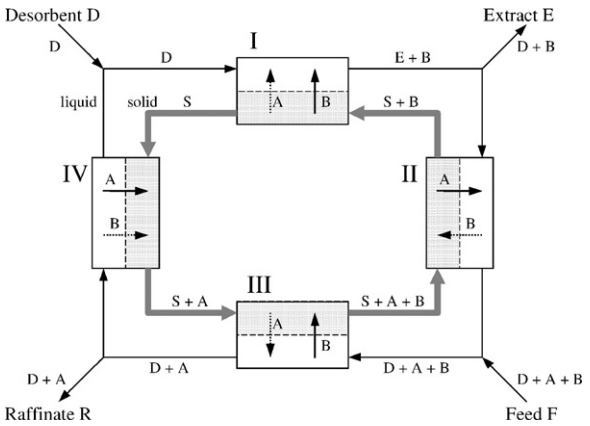

Fig. 1. Equivalent counter-current representation of a simulated moving bed process for separation of a mixture with two species A and B – material flows and adsorption–desorption phenomena in each section.

In this study, experiments were conducted in the Max-Planck-Institut Dynamik Komplexer Technisher Systeme in Magdeburg (Germany) on a preparative SMB unit (CSEP C912, Knauer, Berlin, Germany). Fig. 2 shows a schematic representation of this unit. Contrary to usual configurations where the inlet and outlet ports are switched, the columns, connected to a multi-function valve, are switched counter-current to the direction of the fluid flow. This valve consists of a rotor and a stator with 24 ports each. The ports are connected to each other by continuous channels. Hence, all the devices inside the inner circle moves during the switching, whereas, the rest is fixed. Note that this SMB plant is built for up to 12 columns but only 8 columns are introduced in the process used in Magdeburg. The free ports are connected by short capillaries, as described in [14] and the valve switches alternatively one and two times successively during a full cycle (which is equal to 8 switching periods).

The experiments consist in the separation of cyclopentanone and cyclohexanone on 8 columns with 21.2 mm internal diameter and 100 mm length. The stationary phase is a silica gel (LiChroprep RP-18, particle size 25–40 μm, Merck, Darmstadt) and the solvent is a water/methanol solution (70/30).

The process is equipped with two inlet pumps, one on the feed flow (P4), and another on desorbent flow (P3). Two other pumps

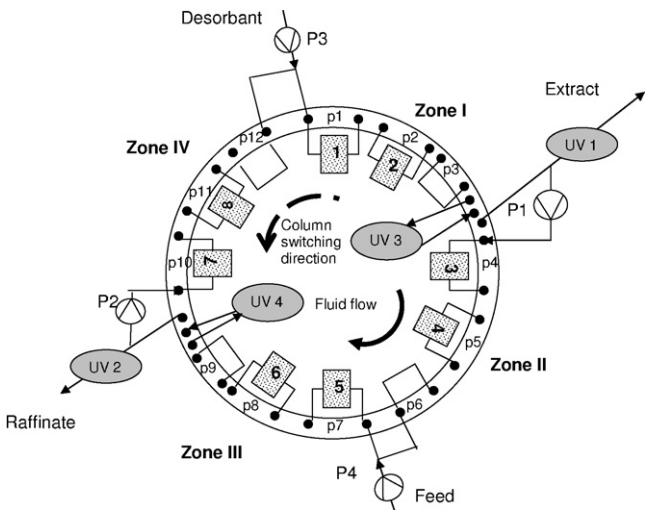

Fig. 2. Schematic representation of the Knauer CSEP C912 unit (Max Planck Institute, Magdeburg, Germany) with 8 columns (position at start-up).

are located in the circulating stream (P1 and P2). Besides, this SMB process is also equipped with four UV detectors, two in the circulating stream (UV3 and UV4) and two on the product outlets (UV1 and UV2). They have been calibrated by injecting successive step changes of known concentration of cyclopentanone and cyclohexanone. In this study, it turns out that, in the considered concentration range, the UV signal is equal to a weighted sum of the concentration of both products.

The following conventions will be used in the paper:

- the columns are numbered ($m = 1, \ldots, 8$); at the start-up, column 1 follows the desorbent input; column number 2 is the following in the direction of the fluid flow, and so on;
- a position (p) is defined as a place dedicated to the columns in the SMB unit; some are really occupied by a column, others by a capillary replacing the column.

Columns move when the valve rotates whereas positions are fixed.

3. Parameter identification from batch experiments

3.1. Introduction

In this section, the method to determine the parameters of a SMB model from elution peaks developed in [13] is transposed to the studied separation. The experiments are performed directly on the columns of the SMB process. Indeed, as it will be explained in Section 3.4, it is more advisable to work directly with experimental data recorded on the SMB columns and not on analytical columns to ensure that the porosity used in the estimation of the isotherm parameters is the same as the porosity of the SMB. Moreover, it is assumed that all the columns of the SMB unit have the same properties and hence the same parameters. Therefore, identification is performed from experiments on one of the SMB columns only. This hypothesis will be discussed in Section 5.

Hereafter, the description of the experiments is given before the modelling of the elution experiments. Then, the set of parameters to be identified by an optimization method is presented. The statement and the solution of the identification problem follow. Finally, parameter estimation is performed from batch data.

3.2. Batch experiments

In our particular case, column 2 which is followed by the detector UV3 is chosen for the batch experiments. By rotating the valve, it is placed after pump P3 (cf. Fig. 2). A mixture of cyclopentanone (the less retained component, called A) and cyclohexanone (the most adsorbed component, called B) is introduced in the column thanks to a manual injection valve associated to pump P3. Elution peaks are measured at the end of the column with detector UV3.

To reproduce the conditions of enantiomer separations, the injected concentration of component A is equal to the injected concentration of component B.

Two data sets are used for each parameter estimation, one resulting from an injection at low concentration, called S_1, the other from an injection at high concentration, called S_2. The injected concentrations are prepared volumetrically by the user. The smallest concentration has been chosen high enough to be detectable and the highest concentration to be below the limit of solubility. The flow rate and the injected volume are the same for each experiment.

Letting $y^{mes}_{S_\ell}(t), \quad \ell = 1, 2$, denote the measured signal associated to the input concentration $c_{F,i,\ell}$, $i = A, B$, the data set S_ℓ can be defined by

$$S_\ell = \{y^{mes}_{S_\ell}(t_\ell(h)), \quad h = 0, 1, \ldots, M_\ell - 1, \quad t_\ell(h) < t_\ell(h+1)\}$$

where the injection is assumed to take place at time $t = t_\ell(0)$. M_ℓ is the number of measurements in data set S_ℓ.

3.3. Modelling of an elution experiment

In this section, the model equations necessary to simulate an elution experiment are presented. First the column model and the inlet concentration profile are described. Then the isotherm model is presented and finally the measurement equation which reproduces the information given by the sensor is given.

3.3.1. Column model and inlet concentration profile

As already explained in the introduction, a systematic comparison of the computational load and the identifiability of the parameters for the linear-driving force (LDF), the equilibrium dispersive and the kinetic model has been reported in [13]. From this study, it follows that the kinetic model yields an appropriate compromise between these criteria. Hence this model is retained here.

The equations of the kinetic model for a chromatographic column are written as follows for the liquid phase:

$$\frac{\partial c_i}{\partial t} = -v\frac{\partial c_i}{\partial z} - \frac{1-\varepsilon}{\varepsilon}\frac{\partial q_i}{\partial t} \tag{1}$$

with c_i, the fluid concentration; q_i, the solid concentration; v, the fluid velocity; ε, the porosity. t denotes the time and z, the axial coordinate. $i = A, B$ refers to the species in the mixture to separate.

For the solid phase, the mass balance is given by:

$$\frac{\partial q_i}{\partial t} = k_i^{rel} v (q_i^{eq} - q_i) \tag{2}$$

with k_i^{rel}, the relative mass transfer coefficient, and q_i^{eq}, the adsorbed equilibrium concentration.

The ideal shape of the inlet concentration profile should be a rectangle but dispersion phenomena affect significantly the profile. In this study, the inlet concentration profile is described as follows:

If $t < t_{d_{in}}$ then

$$u_i(t) = 0$$

else
if $t < (t_p + t_{d_{in}})$ then

$$u_i(t) = c_{F,i}\left(1 - \exp\left(\frac{-(t - t_{d_{in}})}{t_{tr}}\right)\right)$$

else

$$u_i(t) = c_{F,i}\left(1 - \exp\left(\frac{-(t - t_{d_{in}})}{t_{tr}}\right)\right) - c_{F,i}\left(1 - \exp\left(\frac{-((t - t_{d_{in}}) - t_p)}{t_{tr}}\right)\right) \tag{3}$$

with $c_{F,i}$, the injected concentration of component i, $i = A, B$, t_p, the injection duration and t_{tr}, a constant characterizing the rise time of the pulse. $t_{d_{in}}$ is the time delay due to the dead volume between the injection pump and the SMB process, $t_{d_{in}} = V_{d_{in}}/Q$ with $V_{d_{in}}$, the dead volume located before the column and Q, the feed flow rate. It is implicitly assumed that injection starts at $t = 0$ s.

3.3.2. Isotherm model

The adsorbed equilibrium concentration is related to the liquid-phase concentration by an adsorption equilibrium relation. Many multicomponent non-linear isotherm equations have been described. As the type of isotherm equation is not *a priori* known

in this study, the obvious first choice is the competitive Langmuir isotherm. The corresponding equation is the following:

$$q_i^{eq} = \frac{q_{Si} b_i c_i}{1 + b_A c_A + b_B c_B} \tag{4}$$

where q_{Si} and b_i are respectively the saturation capacity and the equilibrium constant of component i, $i = A, B$.

Note that at infinite dilution, the Langmuir isotherm reduces to a linear relation with slope H_i, where $H_i = q_{Si} b_i$.

3.3.3. Measurement equation

As already explained, the data are collected at the end of the column with a UV detector. In this study, the resulting UV signal is a weighted sum of the concentration of the two products. Letting $c_i(t, z, c_{F,i,\ell})$, denote the solution of Eqs. (1), (2), (4) for input (3), for data set S_ℓ, $\ell = 1, 2$, the measurement equation, reproducing the information given by the sensor, can be written:

$$y_{S_\ell}(t) = c_A(t, L, c_{F,i,\ell}) UV(A) + c_B(t, L, c_{F,i,\ell}) UV(B) \tag{5}$$

where L is the column length. $UV(A)$ ($UV(B)$) is the calibration coefficient of component A (B). It is easily determined by injecting successive step changes of known concentration of component A (B).

3.4. Unknown parameters

In Eqs. (1)–(5), the parameters are the fluid velocity, the porosity, the mass transfer coefficients, the injected concentrations, the injected volume, the dead volume, the isotherm parameters and the UV calibration coefficients. The velocity is obtained from the fluid flow rate. The porosity is calculated as described in [15] by using the elution peak of a non-retained product (a solution of thiocarbanide). The injected concentrations are chosen by the user. Note that even if the injected concentrations are chosen equal for component A and B, both concentrations are considered separately in this study as they are prepared independently and thus affected by uncorrelated errors. The injected volume is defined by the volume of the injection valve. The dead volume is a known process characteristic. The UV calibration coefficients are obtained from simple experiments [16]. All these known parameters will be gathered in the vector $\zeta(k)$: $\zeta(k) = [Q \;\; V_{inj} \;\; c_{F,A}(k) \;\; c_{F,B}(k) \;\; UV(A) \;\; UV(B) \;\; \varepsilon \;\; V_{d_{in}}]^T$, $k = 1, \ldots, M_T$. As two experiments are performed with different process working modes, which differ, in this study, by the injected concentrations, this vector of parameters is a function of the measurement point k through $c_{F,i}(k) = c_{F,i,1}$ for $k = 1, \ldots, M_1$ and $c_{F,i}(k) = c_{F,i,2}$ for $k = M_1 + 1, \ldots, M_T$, $i = A, B$. The vector $\zeta_v = \left[\zeta(1)^T \; \ldots \; \zeta(M_T)^T \right]^T$ will also be used subsequently. The estimated value obtained from simple experiments is called $\hat{\zeta}_v = \left[\hat{\zeta}(1)^T \; \ldots \; \hat{\zeta}(M_T)^T \right]^T$.

The parameters are now grouped into two classes, those which can be assumed to be perfectly known and those which are subject to an estimation error. $V_{d_{in}}$, the dead volume, is assumed to be known without error as it is a known process characteristic. The other elements of $\zeta(k)$, $k = 1, \ldots, M_T$, may be corrupted by some errors. Indeed, for example, the precision of the pump is limited or the measurement of the calibration coefficients may not be performed without error. However, as the batch experiments are performed on one SMB column, the porosity is also supposed to be known without error. Indeed, in [17], it is demonstrated that, if erroneous porosity is used in the determination of the isotherm parameters from batch experiments, these parameters will not be correctly estimated but they will nevertheless be able to describe quite accurately the propagation of the elution fronts. Hence, in this study, the error on the porosity will be neglected during the identification of the unknown parameters from one SMB column. Consequently, for the identification step, two vectors will be used:

- one containing the parameters assumed to be known without error: $\zeta_{we} = [V_{d_{in}} \;\; \varepsilon]^T$;
- another with the parameters which may be corrupted by some errors: $\zeta_e(k) = [Q \; V_{inj} \; c_{F,A}(k) \; c_{F,B}(k) \; UV(A) \; UV(B)]^T$, $k = 1, \ldots, M_T$. The vector $\zeta_{e_v} = \left[\zeta_e(1)^T \; \ldots \; \zeta_e(M_T)^T \right]^T$ will also be used subsequently.

Hence, $\zeta(k) = [\zeta_e(k)^T \;\; \zeta_{we}^T]^T$, $k = 1, \ldots, M_T$.

The other parameters, namely the mass transfer coefficients and the isotherm parameters, are identified following the method described in [13]. The vector of identified parameters is defined as $\theta = [\, k_A^{rel} \;\; k_B^{rel} \;\; H_A \;\; H_B \;\; b_A \;\; b_B \,]^T$.

In order to introduce the dependence on θ and ζ_v, the simulated outputs, resulting from Eq. (5), will be: $y_{S_\ell}(t, \theta, \hat{\zeta}_v)$.

In the following, the measurements and the simulations will be gathered in vectors of length M_T, $M_T = \sum_{\ell=1}^{2} M_\ell$:

$y^{mes} = [\, y_{S_1}^{mes^T} \;\; y_{S_2}^{mes^T} \,]^T$ where $y_{S_\ell}^{mes} = [\, y_{S_\ell}^{mes}(t_\ell(0)) \ldots y_{S_\ell}^{mes}(t_\ell(M_\ell - 1)) \,]^T$ with $\ell = 1, 2$, and $y(\theta, \hat{\zeta}_v) = [\, y_1(\theta, \hat{\zeta}_v(1 : M_1))^T \;\; y_2(\theta, \hat{\zeta}_v(1 + M_1 : M_T))^T \,]^T$ where $y_1(\theta, \hat{\zeta}_v) = [\, y_{S_1}(t_1(0), \theta, \hat{\zeta}(1)) \ldots y_{S_1}(t_1(M_1 - 1), \theta, \hat{\zeta}(M_1)) \,]^T$ and $y_2(\theta, \hat{\zeta}_v) = [\, y_{S_2}(t_2(0), \theta, \hat{\zeta}(M_1 + 1)) \ldots y_{S_2}(t_2(M_2 - 1), \theta, \hat{\zeta}(M_T)) \,]^T$.

$t_\ell(h) < t_\ell(h + 1)$, and $h = 0, 1, \ldots, M_{\ell-1}$. Hence the k^{th} measurement used for identification is labelled: $y^{mes}(k)$ and the k^{th} element of vector $y(\theta, \hat{\zeta}_v)$ is labelled $y(k, \theta, \hat{\zeta}(k))$, where $k = 1, \ldots, M_T$.

3.5. Statement of the identification problem

As described in [13], the unknown parameters are determined by minimizing a measure of the deviation between the experimental profiles and the profiles simulated with the chromatographic model.

The latter are obtained by solving numerically Eqs. (1)–(4) following the method of lines [18]. First, the spatial operators are approximated using a finite difference scheme on a spatial grid. Then the resulting system of semi-discrete ODEs is integrated in time [6]. The solution is introduced in the measurement Eq. (5) to give the simulated measurement signal. Solutions obtained for both data sets are introduced in a vector $y(\theta, \hat{\zeta}_v)$, as proposed in Section 3.4.

To specify the parameter estimation problem, it is necessary to describe the constraints on the parameters and the cost functions.

For each unknown parameter, the prior knowledge allows one to specify an interval within which the estimated value must lie: $\theta(j)_{inf} < \theta(j) < \theta(j)_{sup}$. To enforce these constraints, the following non-linear transformation is performed on each parameter [19]:

$$\theta(j) = 0.5(\theta(j)_{\sup} + \theta(j)_{\inf} + (\theta(j)_{\sup} - \theta(j)_{\inf}) \tanh(\theta^*(j))) \tag{6}$$

with $\theta(j)$, the j^{th} parameter to identify, and $\theta^*(j) \in \Re$, the parameter which is actually determined by numerical optimization. This way, an unconstrained optimization problem results, which can be solved using the technique presented in Section 3.6 below. Note that, for simplicity, by an abuse of notation, $y(\theta, \zeta_v)$ is written $y(\theta^*, \zeta_v)$ after parameter transformation.

Two cost functions are considered. The first one is defined as:

$$J^{cl}(\theta^*, \hat{\zeta}_v) = \sum_{k=1}^{M_1} C_1 (y^{mes}(k) - y(k, \theta^*, \hat{\zeta}(k)))^2 + \sum_{k=M_1+1}^{M_2} (y^{mes}(k) - y(k, \theta^*, \hat{\zeta}(k)))^2 \quad (7)$$

with $y^{mes}(k)$, the k^{th} measurement value, $y(k, \theta^*, \hat{\zeta}(k))$, the corresponding model ouput prediction, and M_ℓ, the number of measurements of the data set S_ℓ, $\ell = 1, 2$. C_1 is a constant that ensures that each data set has the same importance in the cost function: $C_1 = \max(y^{mes}_{S_2})/\max(y^{mes}_{S_1})$.

The second cost function helps considering the output error in a relative sense [16]:

$$J^{ln}(\theta^*, \hat{\zeta}_v) = \sum_{k=1}^{M_1} R_1 (\ln(y^{mes}(k)) - \ln(y(k, \theta^*, \hat{\zeta}(k))))^2 + \sum_{k=M_1+1}^{M_2} (\ln(y^{mes}(k)) - \ln(y(k, \theta^*, \hat{\zeta}(k))))^2 \quad (8)$$

R_1 is a constant that ensures that each data set has the same importance in the cost function: $R_1 = \max(\ln(y^{mes}_{S_2}))/\max(\ln(y^{mes}_{S_1}))$.

Note that, to avoid having an infinite value of the cost function when using expression (8), a lower bound saturation of the values of $y^{mes}(k)$ and of $y(k, \theta^*, \hat{\zeta}(k))$ is performed:

if $y^{mes}(k) < y_{sat}$, $y^{mes}(k) = y_{sat}$

or if $y(k, \hat{\theta}^*, \hat{\zeta}(k)) < y_{sat}$ $y(k, \hat{\theta}^*, \hat{\zeta}(k)) = y_{sat}$

where $y_{sat} > 0$.

The results obtained with both cost functions will be compared in the following.

3.6. Solution of the parameter estimation problem

In this section, the optimization method and the identification procedure are first presented. The calculation of the confidence interval follows.

3.6.1. Optimization method

The optimization method used in this study is an algorithm for unconstrained optimization by quadratic approximation developed by Powell and called UOBYQA [20].

3.6.2. Multistart procedure

A multistart procedure is executed to alleviate the problem of local minima. It consists in performing 2^n identification runs, with n, the number of parameters. Each run corresponds to a different initial value of the estimated parameter vector, θ_0^{*r} ($r = 1, \ldots, 2^n$). The latter are calculated after the following steps:

1. $\hat{\theta}_{init}$, a rough approximation of the parameters, is obtained from classical experimental method selected in [13] applied directly on data set S_1 and S_2;
2. $\Delta\hat{\theta}_{init}$, an upper bound of the error on $\hat{\theta}_{init}$, is estimated as described in [21];
3. θ_0^r, $r = 1, \ldots, 2^n$ corresponds to the vertices of a hyper-parallelepiped centred around $\hat{\theta}_{init}$ with edge length equal to 2 $\Delta\hat{\theta}_{init}$;
4. θ_0^{*r} is obtained by parameter transformation (6) of θ_0^r.

Each identification run yields an estimated parameter value denoted $\hat{\theta}^{*r}$, or after transformation by Eq. (6), $\hat{\theta}^r$, $r = 1, \ldots, 2^n$. The associated value of the minimum cost function will be denoted $J^r_{\min}$, $r = 1, \ldots, 2^n$. Next J_{min} is calculated from $\min_r J^r_{\min}$ and $\hat{\theta}_{\min}$ is the parameter value for which J_{min} is reached. As it corresponds to the smallest cost function obtained, $\hat{\theta}_{\min}$ is used subsequently for validation tests.

3.6.3. Confidence interval

The confidence interval on the estimated parameters, $\hat{\theta}^*_{\min}$, is estimated taking the error on the a-priori estimated parameter $\hat{\zeta}_v$ into account. To this end, the calculation of the covariance matrix on the basis of the asymptotical theory [22] is adapted. The development has been presented in [16] and a brief summary is given in Appendix A. The estimation of the covariance matrix of the parameter error is calculated as follows:

$$Cov = \hat{E}(\tilde{\theta}^* \tilde{\theta}^{*T}) = \hat{P}_{M_T} \frac{J_{\min}(\hat{\theta}^*, \hat{\zeta}_v) - \Psi + \Lambda + \Phi}{M_T - \sum_{k=1}^{M_T} g^T_{\theta^*}(k, \hat{\theta}^*, \hat{\zeta}_e(k)) \hat{P}_{M_T} g_{\theta^*}(k, \hat{\theta}^*, \hat{\zeta}_e(k))} + \Omega \quad (9)$$

where

$$\Psi = 2 \sum_{k=1}^{M_T} \sum_{k^*=1}^{M_T} g^T_{\zeta_e(k^*)}(k^*, \hat{\theta}^*, \hat{\zeta}_e(k^*)) Q^{\zeta_e}(k^*, k) g_{\zeta_e(k)}(k^*, \hat{\theta}^*, \hat{\zeta}_e(k^*)) w(k^*)$$

$$\Lambda = \sum_{k=1}^{M_T} \sum_{k'=1}^{M_T} \sum_{k^*=1}^{M_T} g^T_{\zeta_e(k)}(k^*, \hat{\theta}^*, \hat{\zeta}_e(k^*)) Q^{\zeta_e}(k, k') g_{\zeta_e(k')}(k^*, \hat{\theta}^*, \hat{\zeta}_e(k^*)) w(k^*)$$

$$\Phi = \sum_{k^*=1}^{M_T} g^T_{\theta^*}(k^*, \hat{\theta}^*, \hat{\zeta}_e(k^*)) \hat{P}_{M_T} \left[\sum_{k'=1}^{M_T} \sum_{k=1}^{M_T} g_{\theta^*}(k, \hat{\theta}^*, \hat{\zeta}_e(k)) w(k) g^T_{\zeta_e(k)}(k, \hat{\theta}^*, \hat{\zeta}_e(k)) Q^{\zeta_e}(k, k') g_{\zeta_e(k')}(k', \hat{\theta}^*, \hat{\zeta}_e(k')) w(k') g^T_{\theta^*}(k', \hat{\theta}^*, \hat{\zeta}_e(k')) \right] \hat{P}_{M_T} g_{\theta^*}(k^*, \hat{\theta}^*, \hat{\zeta}_e(k^*))$$

$$\Omega = \hat{P}_{M_T} \left[\sum_{k'=1}^{M_T} \sum_{k=1}^{M_T} g_{\theta^*}(k, \hat{\theta}^*, \hat{\zeta}_e(k)) w(k) g^T_{\zeta_e(k)}(k, \hat{\theta}^*, \hat{\zeta}_e(k)) Q^{\zeta_e}(k, k') g_{\zeta_e(k')}(k', \hat{\theta}^*, \hat{\zeta}_e(k')) w(k') g^T_{\theta^*}(k', \hat{\theta}^*, \hat{\zeta}_e(k')) \right] \hat{P}_{M_T}$$

with $\tilde{\theta}$, the estimation error: $\tilde{\theta}^* = \hat{\theta}^* - \theta^*_{tr}$, θ^*_{tr}, the true value of the parameter,

$$g_{\theta^*}(k, \theta^*, \zeta_e(k)) = \frac{\partial y(k, \theta^*, \zeta_e(k))}{\partial \theta^*},$$

$$g_{\zeta_e(k)}(k, \theta^*, \zeta_e(k)) = \frac{\partial y(k, \theta^*, \zeta_e(k))}{\partial \zeta_e(k)}$$

Table 1
Separation and experimental set-up characteristics.

ε	UV(A)	UV(B)	C_1	$t_{d_{in}}$ (s)	Flowrate Q (ml/min)	t_{tr} (s)	$c_{F,A,1} = c_{F,B,1}$ (vol%)	$c_{F,A,2} = c_{F,B,2}$ (vol%)	Injected volume (ml)
0.6	0.1991	0.1919	41.31	20	30	0.1	0.12	6	2

Table 2
Batch identification conditions.

$\hat{\theta}_{init}$	$\Delta\hat{\theta}_{init}/\hat{\theta}_{init}$	θ_{inf}	θ_{sup}	y_{sat}	C_1	R_1	M_1	M_2
1466 1015 3 6.96 0.24 0.56	0.3 0.3 0.1 0.1 0.3 0.3	0 0 0 0 0 0	4235 4235 10 10 1 1	1e−3	41.3	3	316	455

$$k = 1, \ldots, M_T. \quad \hat{P}_{M_T}^{-1} = \sum_{k=1}^{M_T} g_{\theta^*}(k, \hat{\theta}^*, \hat{\zeta}_e(k)) g_{\theta^*}^T(k, \hat{\theta}^*, \hat{\zeta}_e(k)) w(k).$$

The covariance matrix of the error on the estimate of $\hat{\zeta}_e(k)$ is called $Q^{\zeta_e}(k, k')$. $w(k)$ corresponds to the weighting factors. For the cost function J^{cl}, $w(k) = \sqrt{C_1}$ for $k \le M_1$ and $w(k) = 1$ for $k > M_1$. For the cost function J^{ln}, $w(k) = \sqrt{R_1}$ for $k \le M_1$ and $w(k) = 1$ for $k > M_1$.

Hence, the confidence interval at 65% on $\hat{\theta}^*(j)$, the j^{th} component of $\hat{\theta}^*$ ($j = 1, \ldots, n$), is calculated as: $\hat{\theta}^*(j) \pm \sqrt{Cov(j, j)}$. Then, transformation (6) is applied to find the confidence intervals on $\hat{\theta}(j)$.

3.7. Batch identification from experiments

In this section, the results of the identification from batch experiments performed on the plant described in Section 2 are presented.

Table 1 gives the separation and set-up characteristics for the realized elution experiments and Table 2 shows the identification conditions.

The following notations are now introduced: $\hat{\theta}_{\min}$ represents the parameter identified with the cost function J^{cl} and $\hat{\theta}_{\min}^{\ln}$ the parameter identified with the cost function J^{ln}. The results of the identification performed with the two cost functions J^{cl} and J^{ln} are shown in Table 3. Both cost functions J^{cl} and J^{ln} give very similar results for parameters $\hat{H}_{i\,\min}$ and $\hat{b}_{i\,\min}$, $i = A, B$, whereas, parameters $\hat{k}_{i\,\min}^{rel}$ are significantly different. Moreover, the identified parameters corresponding to the linear part of the isotherm and describing the behaviour at low concentration, $\hat{H}_{A\,\min}$ and $\hat{H}_{B\,\min}$, are close to the initial ones, $\hat{H}_{A\,init}$ and $\hat{H}_{B\,init}$.

Figs. 3 and 4 show the experimental profiles as well as the peaks simulated with $\hat{\theta}_{init}$ and with $\hat{\theta}_{\min}$ for both cost functions. Note that data sets, S_1 and S_2 used together for identification, are shown here separately for sake of clarity. These figures help to validate our identification approach. Note that the simulations are only compared with data that have been used for parameter estimation. It should be interesting to validate the method with other experimental sets, but, unfortunately, data recorded at other process working modes are not available. Nevertheless, the method will be validated with SMB experiments.

Table 3
Batch identification results $J_{init}^{cl}/(M_1 + M_2) = 1.2\text{e}-4$; $J_{\min}^{cl}/(M_1 + M_2) = 2.81\text{e}-5$; $J_{init}^{\ln}/(M_1 + M_2) = 4.14$; $J_{\min}^{\ln}/(M_1 + M_2) = 6.7\text{e}-2$.

	$\hat{\theta}_{init}$	$\hat{\theta}_{\min}$	$\hat{\theta}_{\min}^{\ln}$
k_A^{rel} (m^{-1})	1466	1546	953.1
k_B^{rel} (m^{-1})	1015	1000.8	720.1
H_A	3	3.05	3.075
H_B	6.96	7.1	7.09
b_A (vol%)$^{-1}$	0.24	0.215	0.21
b_B (vol%)$^{-1}$	0.56	0.66	0.65

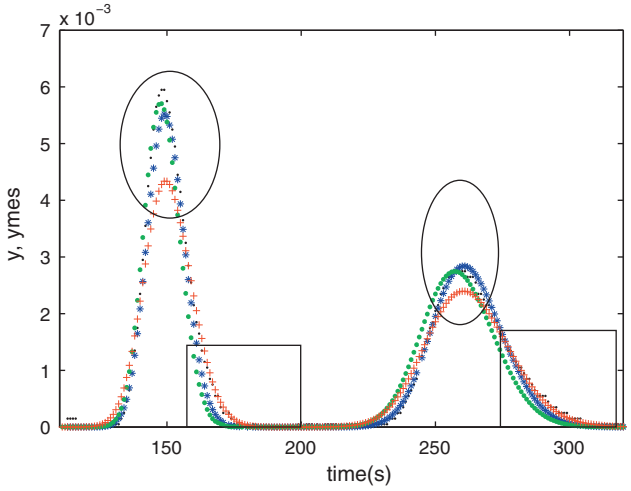

Fig. 3. Results of parameter estimation for column 2 with data set S_1; ••• experimental profile; ✻✻✻ $y(k, \hat{\theta}_{\min}, \hat{\zeta}(k))$; +++ $y(k, \hat{\theta}_{\min}^{\ln}, \hat{\zeta}(k))$; ●● $y(k, \hat{\theta}_{init}, \hat{\zeta}(k))$, $k = 1, \ldots, M_1$.

The simulated profiles obtained with the parameters identified with J^{cl} are different from those simulated with the parameters estimated with J^{ln}. On the one hand, in general, the cost function J^{ln} gives profiles for which the bottom of the desorption fronts (as seen in the rectangles) are close to the experimental profiles. However, the top of the peaks (as seen in the circles) is not well reproduced at low concentration (data set S_1). On the other hand, results obtained with cost function J^{cl} provide peaks with a general shape (height and position) similar to the experimental ones, although the shape of the desorption fronts obtained with cost function J^{ln} is better. The good reproduction of the shape of the fronts may be a advantage in SMB processes for control methods based on the position of the fronts. However, at this stage, it is difficult to conclude from batch experiments. Results must be compared in SMB mode.

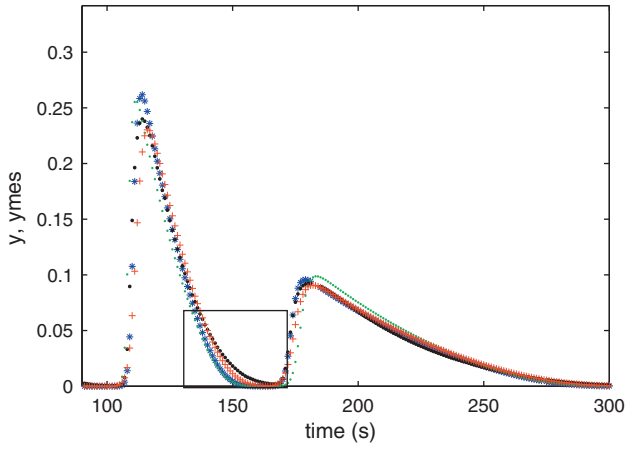

Fig. 4. Results of parameter estimation for column 2 with data set S_2; ••• experimental profile; ✻✻✻ $y(k, \hat{\theta}_{\min}, \hat{\zeta}(k))$; +++ $y(k, \hat{\theta}_{\min}^{\ln}, \hat{\zeta}(k))$; ●● $y(k, \hat{\theta}_{init}, \hat{\zeta}(k))$, $k = 1, \ldots, M_1$.

Table 4
Upper bounds of the confidence intervals (65%).

	Cost function J^{cl}	Cost function J^{ln}
k_A^{rel} (m^{-1})	[266; 3515]	[677; 1296]
k_B^{rel} (m^{-1})	[84; 3473]	[508; 974]
H_A	[2.8; 3.27]	[3; 3.15]
H_B	[6.4; 7.7]	[6.9; 7.3]
b_A (vol%)$^{-1}$	[0.13; 0.32]	[0.13; 0.3]
b_B (vol%)$^{-1}$	[0.32; 0.89]	[0.49; 0.78]

The upper bounds of the confidence intervals at 65% are given in Table 4 for both cost functions. Details about the estimation of $Q^{\zeta e}$ are given in appendix 8.2. of [16]. The confidence intervals are larger for the cost function J^{cl} than for the cost function J^{ln}. However, the intervals are probably overestimated. It is possibly due to the numerous assumptions performed to obtain Eq. (9), notably a number of samples that tends to infinity (cf. Appendix A). As batch elution profiles are less sensitive to the mass transfer coefficients, the confidence interval is larger for the mass transfer coefficients than for isotherm parameters.

4. SMB modelling

In this section, the modelling of the SMB processes is discussed in order to build the model that will be used to validate the identification approach. The simulation results and SMB experiments will be compared in Section 5 in order to verify whether the parameters identified from batch experiments may be used in a SMB model

In the experiments and simulations considered in the SMB operating mode, the start-up of the plant coincides with the beginning of the injection of continuous feed flow in the process filled with solvent. Each experiment is performed with fixed working conditions (constant injected concentrations, constant flow rates and constant switching time).

First of all, the model of a SMB column is considered. Next, the switching mechanism is modelled as well as the dead volumes within the process. Finally, the inlet concentration profile and the measurement equations are described.

4.1. Column modelling

To perform the validation, a SMB kinetic model is needed. For each column of the SMB plant, Eqs. (1), (2) and (4) are valid.

4.2. Switching

For simplicity, the fixed referential is associated to the columns. Hence, the switching is modelled by the movement of the inlet and outlet ports and hence by the change of the flow rate in each column. To perform this, a vector which contains the flow rate in each column is defined: $Q = [\, Q_1 \ \ldots \ Q_8 \,]$.

At the start-up,

$$Q_1^0 = Q_2^0 = Q_I; \quad Q_3^0 = Q_4^0 = Q_{II}; \quad Q_5^0 = Q_6^0 = Q_{III};$$

$$Q_7^0 = Q_8^0 = Q_{IV} \quad \text{with} \quad Q_{III} = Q_{II} + Q_F \quad \text{and} \quad Q_I = Q_{IV} + Q_S$$

where Q_z is the flow rate in zone z, $z = I, \ldots, IV$, Q_F, the feed flow rate and Q_S, the solvent flow rate.

Valve switching is taken into account by considering that the flowrate in column m during a switching period is equal to the flowrate in column $m-1$ during the previous period:

$$Q_m^{n_s} = Q_{m-1}^{n_s-1} \tag{10}$$

where n_s denotes the number of switches performed since the start-up. The velocity in column m is recalculated from Q_m after each switching for use in Eqs. (1) and (2).

4.3. Extra-column dead volumes modelling

4.3.1. General equation

As explained in [2,7,9], it is important to model the dead volumes introduced by the valves, the connecting tubes and the pumps. It is especially the case in this experimental set up where some pumps, UV detectors, capillaries replacing columns and long connections are placed in the circulating loop between the columns (cf. Fig. 2).

The mass balance equation for component i, $i = A, B$, in the dead volume d is calculated as follows [9]:

$$\frac{\partial c_{i,d}}{\partial t} = -v_d \frac{\partial c_{i,d}}{\partial z_d} + D_d \frac{\partial^2 c_{i,d}}{\partial {z_d}^2}. \tag{11}$$

with v_d, the velocity in dead volume d; D_d, the diffusion coefficient in dead volume d.

As most of the dead volume consists of tubes where plug flow conditions may be considered, D_d is very small ($\approx$1e−9 m^2/s).

4.3.2. Movement of the dead volumes in the circulating loop

In [9], the dead volume surrounding a column is divided into two parts: one located before the column, another after. However, some dead volumes switch from one section to the other, like the columns, while others stay in the same section all the time. For example, in the studied experimental plant, as seen in Fig. 2, some dead volumes move, as the ones associated to UV3 and UV4 detectors, and others, which are not negligible, as the ones associated to the pumps and their connectors, are fixed. Hence, it is proposed to consider these different behaviours in the model. As seen in Fig. 5, at the n^{th} switching period, the dead volume at position p is divided into four parts, two moving ones, and two fixed ones:

- the dead volume $V_{d,m}^{col,b}$ is located before column m and corresponds to the connection between the valve and column m or to the inside of the valve; this dead volume switches with the column at each sampling time;
- the dead volume $V_{d,m}^{col,af}$ is located after column m and corresponds to the connection between the column m and the valve or to the inside of the valve; this dead volume moves with the column at each sampling time;
- the dead volume $V_{d,p}^{port,b}$ is situated before column m and corresponds to the pumps, P1 and P2, and connections from the inlet ports; this dead volume does not move;
- the dead volume $V_{d,p}^{port,af}$ is situated after column m and corresponds to the connections to the outlet ports or to the pumps P1 and P2; this dead volume does not move.

Hence, if the fixed referential is associated to the columns, the movement of the dead volumes associated to the inlet and outlet ports, $V_{d,p}^{port,b}$ and $V_{d,p}^{port,af}$, is modelled by considering that the concentration profiles in dead volumes $V_{d,p}^{port,b}$ and $V_{d,p}^{port,af}$, at the beginning of a switching interval, are equal to the profiles obtained in the dead volume $V_{d,p-1}^{port,b}$ and $V_{d,p-1}^{port,af}$ at position $p-1$ at the end of the previous period, which gives in each dead volume:

$$c_{i,d,p}(t_s^{n_s} = 0, z_{dp}) = c_{i,d,p-1}({t_s}^{n_s-1} = \Delta t, z_{dp-1}) \tag{12}$$

with $c_{i,d,p}$, the concentration of component i in the dead volume considered at position p. z_d is the axial coordinate in the dead volume. Δt is the switching period and ${t_s}^{n_s}$ is the time elapsed since the ${n_s}^{\text{th}}$ switch.

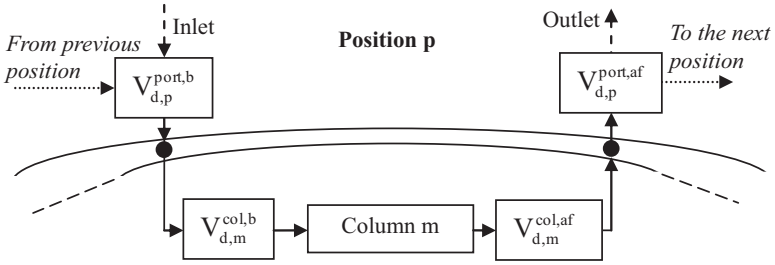

Fig. 5. Schematic representation of the dead volumes surrounding a column in the considered SMB unit.

Note that, as explained in the introduction and illustrated in Fig. 2, there are only 8 columns instead of 12 and the free ports are connected by short capillaries. In this case, if position p is not occupied by a column, $V_{d,m}^{col,b}$ and $V_{d,m}^{col,af}$ are directly connected and include the dead volume of the capillary.

This approach for modelling extra-column dead volumes is validated with experimental data in Section 5.

4.4. Inlet concentration profile

The start-up of the plant coincides with the beginning of the injection of a continuous feed flow in the process filled with solvent. In the inlet concentration profile, a time delay is introduced to take into account the dead volume between the feed tank and the SMB unit. This delay may influence the concentration profiles at start-up and postpone the establishment of the cyclic steady-state. Moreover, the ideal shape of the injection front should be rectangular but dispersion phenomena significantly affect the profile. Hence, the inlet concentration profile of component i, $i = A, B$, can be described as follows:

$$\begin{aligned} &\text{if} \quad t < t_{d_{in}} \\ &\quad u_i(t) = 0 \\ &\quad \text{else} \\ u_i(t) &= c_{F,i}(1 - \exp(-(t - t_{d_{in}})/t_{tr})) \end{aligned} \tag{13}$$

where $t_{d_{in}} = V_{d_{in}}/Q_F$ with Q_F, the feed flow and $V_{d_{in}}$, the dead volume before the SMB unit. $c_{F,i}$ is the feed concentration of component i, $i = A, B$.

4.5. Boundary conditions

The boundary conditions in the liquid and solid phase are obtained by expressing simple mass balances and simple advection equations for each component i ($i = A, B$) at the transition between two dead volumes or between a dead volume and a column. They have the same form as those given in [6] for transition between two columns.

4.6. Model parameters

As for the batch case, for each measurement signal, vectors of a-priori known parameters are defined. As the four UV detectors used (see Fig. 2) do not have the same calibration coefficients, four parameter vectors ζ_δ^{SMB}, $\delta = 1, \ldots, 4$, are defined:

$$\zeta_\delta^{SMB} = [Q_I \quad Q_{II} \quad Q_{III} \quad Q_{IV} \quad \Delta t \quad \varepsilon_1 \quad \ldots \quad \varepsilon_{N_C} \quad V_d \quad c_{F,A} \quad c_{F,B} \quad UV_\delta(A) \quad UV_\delta(B)]^T$$

with N_c, the number of columns and $UV_\delta(i)$, the UV calibration coefficient of detector δ for component i, $i = A, B$. V_d is a vector containing the dead volumes of the SMB unit.

4.7. Measurement equations

The measurement equation is written for detector δ, $\delta = 1, \ldots, 4$:

$$\begin{aligned} y_\delta(t, \theta, \zeta_\delta^{SMB}) = {} & c_{A,d}(t, L_d, \theta, \zeta_\delta^{SMB}) UV_\delta(A) \\ & + c_{B,d}(t, L_d, \theta, \zeta_\delta^{SMB}) UV_\delta(B) \end{aligned} \tag{14}$$

with δ, the sensor number, $c_{i,d}$, $i = A, B$, the concentration of component i in the dead volume before the UV detector. L_d is the length of this dead volume.

UV detectors situated on the extract and raffinate outputs are fixed. However, UV3 and UV4 are moving: the first follows the dead volume $V_{d,p}^{col,af}$ after column 2, the second is placed after the dead volume $V_{d,p}^{col,af}$ after column 6.

4.8. Numerical solution of the model equations

Like for the batch equations, Eqs. (1), (2) and (4) with (10) to (13) are solved numerically following the method of lines [18]. First, the spatial operators are approximated using finite difference schemes on a spatial grid. Then the resulting system of semi-discrete ODEs is integrated in time [6].

5. Validation with SMB experiments

In this section, a validation is performed with SMB experiments to verify the effectiveness of the identification method and of the modelling of the movement of the dead volumes. First the parameters identified in Section 3 are introduced in the model described in Section 4 to simulate the behaviour of the SMB process. The obtained concentration profiles are then compared with experimental profiles. Then, a confidence envelope is estimated to evaluate the simulation errors.

5.1. Comparison of concentration profiles

On the one hand, SMB experiments have been performed on the unit described in Section 2 for three operating conditions (case I to III) described in Table 5.

On the other hand, simulations have been performed with $\hat{\theta}_{\min}$ or $\hat{\theta}_{\min}^{ln}$, estimated in Section 3.7 and a-priori known parameter vec-

Table 5
Operating conditions.

Case	I	II	III
Feed concentration (vol%) ($c_{F,A} = c_{F,B}$)	1.456	1.456	0.73
Switching time (s)	150	130	150
Q_{II} (ml/min)	15.6	28.7	15.6
Q_{IV} (ml/min)	17.9	27	17.2
Q_F (ml/min) (feed flow rate)	10.6	8.4	10.6
Q_S (ml/min) (solvent flow rate)	32.5	31.3	32.5

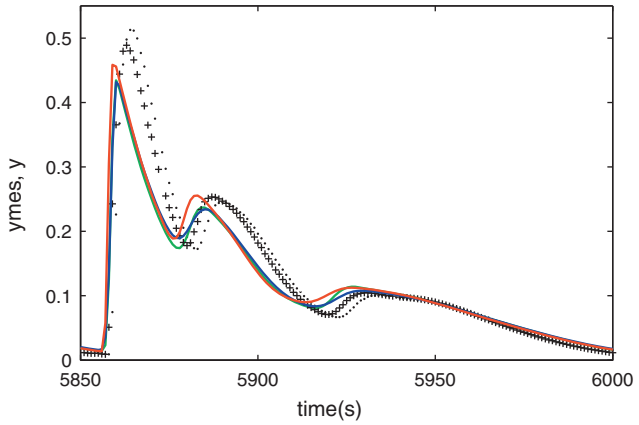

Fig. 6. Case I: UV1 signal (extract); 8th switching period of the 5th cycle; • and +experiments; simulation with the initial parameters; simulation with $\hat{\theta}_{\min}$, simulation with $\hat{\theta}^{\ln}_{\min}$.

tor, $\hat{\xi}^{SMB}_{\delta}$, $\delta = 1, \ldots, 4$. The latter are built from Table 5 which gives the operating conditions, and Tables A.1–A.3 in the appendix which give the UV calibration factors and the values of the dead volumes. The porosities of all the columns are assumed to be equal to the porosity of column 2.

Results of simulations and experiments are, now, compared in order to verify if the parameters determined with batch experiments may be used in a SMB model.

Note that, here, only three operating conditions are considered and all the UV signals corresponding to these operating points are not shown. But similar results have been obtained for the other UV signals and for other operating conditions.

Figs. 6 and 7 show the comparisons between the measurements, the signals simulated with the initial parameter value $\hat{\theta}_{init}$, and with the parameters, $\hat{\theta}_{\min}$ and $\hat{\theta}^{\ln}_{\min}$, identified with the cost function J^{cl} and the cost function J^{ln} respectively. In Fig. 6, the extract signal (UV1) is given for case I. Note that the experiments corresponding to case I have been performed twice in order to check the reproducibility. In Fig. 7, the signal recorded with detector UV3 is represented for case II. Fig. 8 shows the simulated UV3 signal obtained at cyclic steady state for slightly modified flow rates in each section. This study has been performed in order to observe the influence of the precision of the pump on the concentration profiles. Figs. 9 and 10 show the experimental profiles and the results of simulations for different approaches to introduce the dead volumes:

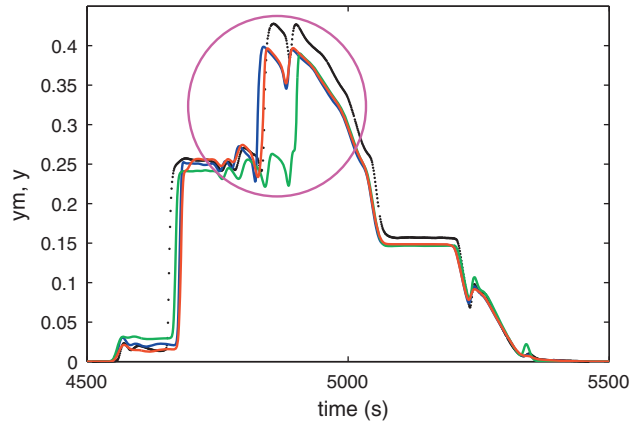

Fig. 7. Case II: detector UV3 signal; from 4th switching period of the 5th cycle; + experiments; simulation with the initial parameters; simulation with $\hat{\theta}_{\min}$; simulation with $\hat{\theta}^{\ln}_{\min}$.

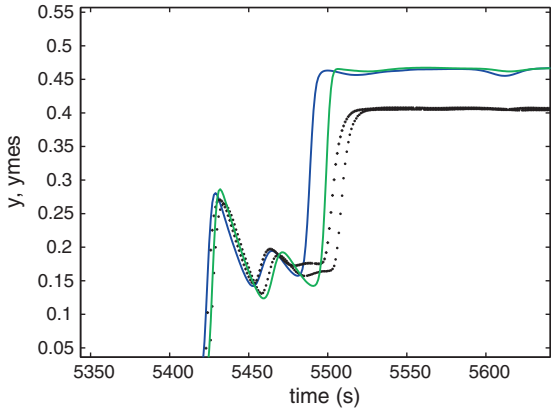

Fig. 8. Case I: detector UV3 signal; 5th switching period of the 4th cycle;• and + experiments; simulation with $\hat{\theta}_{\min}$, simulation with $\hat{\theta}_{\min}$ with modified flow rates (cf. Table 6).

Table 6
Flowrates applied in Fig. 7 (Q: flow rates of case I; Q^{δ}: modified flow rates).

	Q (ml/min)	Q^{δ} (ml/min)	$\Delta Q/Q$ (%)
Zone I	50.4	49.9	1
Zone II	15.6	15.1	3
Zone III	26.2	25.7	2
Zone IV	17.9	17.4	2.3

(a) simulations performed with fixed and mobile dead volumes;
(b) simulations realised with all the dead volumes set to zero;
(c) simulations obtained with all the dead volumes attached to the columns, as considered usually in the literature;
(d) simulations executed with all the dead volumes fixed.

Fig. 10 is a zoom of Fig. 9 on one permutation period.
From these figures, it can be concluded that:

- As seen, in Figs. 9 and 10, the best way to reproduce the amplitude of the concentration signals and the "bumps" in the concentration profiles is to consider that some dead volumes are moving and others are fixed during switching. Moreover, Fig. 9 shows that the change of the amplitude of the extract peak, due to the

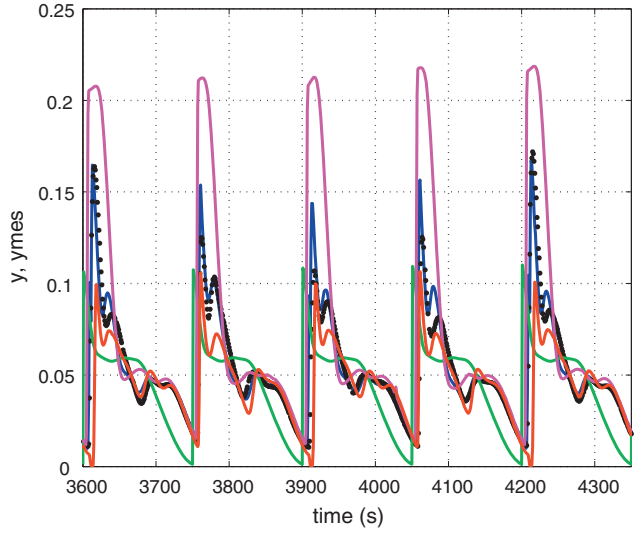

Fig. 9. Case III: UV1 signal (extract); 5 first switching period of the 4th cycle; • experimental signal; simulations with $\hat{\theta}_{\min}$: dead volumes fixed and moving; all the dead volume moving; dead volumes neglected; all the dead volume fixed.

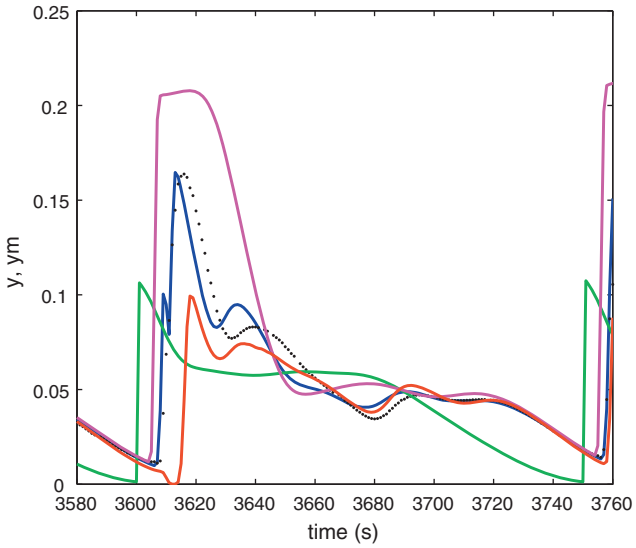

Fig. 10. Case III: UV1 signal (extract); zoom of Fig. 9; • experimental signal; simulations with $\hat{\theta}_{\min}$: dead volumes fixed and moving; all the dead volume moving; dead volumes neglected; all the dead volume fixed.

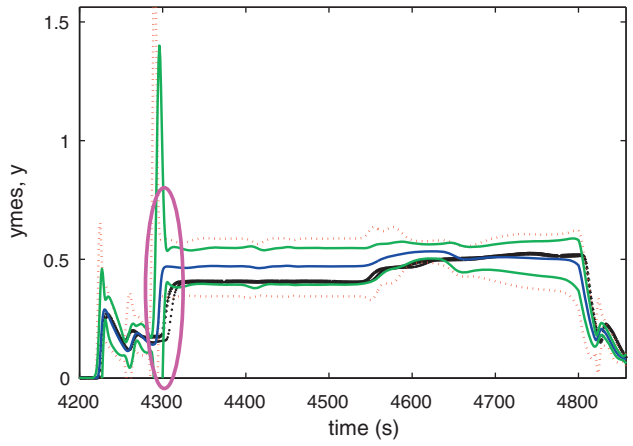

Fig. 11. Case I: detector UV3 signal;* and ··· experiments; simulation with $\hat{\theta}_{\min}$, bounds of the estimated confidence interval with the cost function J^{ln}; bounds of the estimated confidence interval with the cost function J^{cl}.

unequal distribution of the dead volumes in the process, is also well reproduced with fixed and moving dead volume which is not the case with the other configurations. In Fig. 10, where the switching appears at 3600 s, the delay of the apparition of the abrupt front due to the dead volumes is also well reproduced. This validates the approach proposed in Section 4 to model the extra-dead volumes.

- The parameters obtained with cost functions J^{cl} and J^{ln} give similar profiles. As the parameters differ essentially in the value of the mass transfer coefficients, it can be concluded that the latter have a low impact on the SMB concentration profiles studied here.
- In all the figures, the signals simulated with identified parameters give a good approximation of the measurements. The worst parts of the simulation profiles are the fronts of the raffinate signals (cf. Figs. 7 and 8). The differences between the experiments and the simulation results may be explained by different causes:
  - Modelling errors due to the isotherm equations, the choice of boundary conditions [6] and the column model. For the latter, a compromise has to be done. More rigorous models, taking into account the pore diffusion and the axial diffusion like the general rate model, exist [23]. However, the number of parameters is large which increases the difficulty to determine them univocally.
  - Errors in the calibration coefficients or small variations of parameters among the columns.
  - Experimental errors: as shown in Figs. 6 and 8, the reproducibility of the measurements is not perfect and some experimental errors due to inaccuracies in the flow rates or in the preparation of the solutions should also be considered. For example, the largest differences observed in Fig. 8 may be explained by a lack of precision of the flow rates of the SMB plant. Indeed, as seen in Fig. 8, simulation results with smaller internal flow rates (with output and input flows not changed) are closer to the experimental signal.
  - Errors in the modelling of dead volumes where plug flow is assumed.
  - Errors in the values of the dead volumes.
  - Error in the modelling of the permutation which is not abrupt in practice.
- Moreover, the signals simulated with $\hat{\theta}_{\min}$ are close to the one obtained with $\hat{\theta}_{init}$. Indeed, the concentrations obtained at the outputs are not very high and, as already observed in batch, the initial parameters corresponding to the linear part of the isotherm and describing the behaviour at low concentration, $\hat{H}_{A\,init}$ and $\hat{H}_{B\,init}$, are close the identified ones, $\hat{H}_{A\,\min}$ and $\hat{H}_{B\,\min}$. However, a significant improvement of the profile is shown at higher concentration (in the circle in Fig. 7). Indeed parameters b_A and b_B which correspond to the nonlinear behaviour, more important at high concentration, are significantly different after identification.

5.2. Confidence envelope

As seen in the preceding section, the introduction of the identified parameters in a model allows to simulate the behaviour of the process. However as there is an error on the estimated parameters, there is also an error on the results of the simulation:

$$\tilde{y}_\delta(k) = y_\delta(k, \hat{\theta}^*, \hat{\zeta}_\delta^{SMB}) - y_\delta(k, \theta_{tr}^*, \zeta_{\delta\,tr}^{SMB}).$$

with $\zeta_{\delta\,tr}^{SMB}$, the true value of parameter ${\zeta_\delta}^{SMB}$, $\delta = 1, \ldots, 4$.

An upper bound for the confidence envelope may be estimated, as presented in [16], taking the covariance matrix of both $\tilde{\theta}^*$ and $\tilde{\zeta}_\delta^{SMB}$ into account:

$$\hat{E}(\tilde{y}_\delta(k)\tilde{y}_\delta(k)^T)^{up} = \left(\sqrt{ \left.\frac{\partial y_\delta(k,\theta^*,{\zeta_\delta}^{SMB})^T}{\partial\theta^*}\right|_{\theta^*=\hat{\theta}^*,\ {\zeta_\delta}^{SMB}=\hat{\zeta}_\delta^{SMB}} \hat{E}(\tilde{\theta}^*\tilde{\theta}^{*T}) \left.\frac{\partial y_\delta(k,\theta^*,{\zeta_\delta}^{SMB})}{\partial\theta^*}\right|_{\theta^*=\hat{\theta}^*,{\zeta_\delta}^{SMB}=\hat{\zeta}_\delta^{SMB}} } + \sqrt{ \left.\frac{\partial y_\delta(k,\theta^*,{\zeta_\delta}^{SMB})^T}{\partial{\zeta_\delta}^{SMB}}\right|_{\theta^*=\hat{\theta}^*,{\zeta_\delta}^{SMB}=\hat{\zeta}_\delta^{SMB}} Q^{\zeta_e}(k,k) \left.\frac{\partial y_\delta(k,\theta^*,{\zeta_\delta}^{SMB})}{\partial{\zeta_\delta}^{SMB}}\right|_{\theta^*=\hat{\theta}^*,{\zeta_\delta}^{SMB}=\hat{\zeta}_\delta^{SMB}} } \right)^2 \quad k = 1, \ldots, M_T \tag{15}$$

$\hat{E}(\tilde{\theta}^*\tilde{\theta}^{*T})$ is obtained as explained in Section 3.6.3. $Q^{\zeta_e}(k, k)$ is estimated from the knowledge available on the process and experimental estimation error. The upper (lower) bound of the confidence

envelope at 65% is then obtained by adding (subtracting) the quantity $\tilde{y}_\delta(k) = \sqrt{\hat{E}(\tilde{y}_\delta(k)\tilde{y}_\delta(k)^T)^{up}}$ to $y_\delta^{SMB}(k, \hat{\theta}, \hat{\zeta}_\delta^{SMB})$.

Note that, it is supposed that a "true" model exists to apply Eq. (15).

Fig. 11 compares the confidence envelopes for a concentration profile simulated with parameters identified with the cost function J^{ln} and for the cost function J^{cl}.

Some conclusions may be drawn from these plots:

- the confidence envelopes obtained with the cost function J^{ln} are in general smaller than those obtained with the cost function J^{cl};
- the experimental data are, in general, contained in the estimated confidence envelope;
- the largest subset of the experimental data which is not contained in the confidence envelope corresponds to the raffinate fronts (in the pink circle of Fig. 11). As seen in Section 5.1, the latter are poorly simulated;
- the parts of the signal with a larger confidence envelope correspond to parts of the profiles where the reproducibility of the experiments is the worst (in the pink circle of Fig. 11).

6. Conclusions

In this work, a systematic procedure to estimate the isotherm parameters and the mass transfer coefficients of a SMB kinetic model is validated with experimental data. First of all, the parameters are estimated from two elution peaks, one at a small concentration, and another at a higher concentration. The confidence intervals are also estimated for each parameter. Then, these parameters are introduced in a SMB model so as to assess whether the parameters identified from batch experiments may be used in a SMB model. To this end, the introduction of the fixed and moving dead volumes in the SMB model turns out to be necessary. The validation with SMB data is then performed with success.

Hence, the contribution of this work is twofold:

- A systematic procedure to estimate parameters of a SMB model is validated.
- An approach to model dead volumes with fixed and moving parts is proposed.

Both contributions allow simulating the SMB concentration profiles with a good accuracy.

Acknowledgements

The authors are grateful to Achim Kienle and Henning Schramm, Max-Planck-Institut Dynamik Komplexer Technisher Systeme of Magdeburg for their collaboration in the experimental work on the SMB process, and for insightful discussions. Supports from the Walloon Region via the MOVIDA project and from the Belgian Programme on Interuniversity Attraction Poles, initiated by the Belgian Federal Science Policy Office are gratefully acknowledged. The scientific responsibility rests with the authors.

Appendix A. Calculation of the covariance matrix

A summary of the main steps of the calculation of the estimated covariance matrix, $\hat{E}(\tilde{\theta}^*\tilde{\theta}^{*T})$, given in Section 3.6.3, is presented here. The error on the estimate of $\tilde{\zeta}_e(k)$, $k = 1, \ldots, M_T$, is taken into account.

Consider the measurements $y^{mes}(k)$

$$y^{mes}(k) = y(k, \theta_{tr}^*, \zeta_{e_{tr}}(k)) + e(k) \quad k = 1, \ldots, M_T \tag{A.1}$$

with $\zeta_{e_{tr}}(k)$, the true value of the parameter $\zeta_e(k)$.

The error on the estimate of $\hat{\zeta}_e(k)$ is defined as: $\tilde{\zeta}_e(k) = \hat{\zeta}_e(k) - \zeta_{e_{tr}}(k)$

First, some definitions and assumptions are presented:

- The error is zero-mean:

$$E(e(k)) = 0 \quad \forall \quad k \quad \in \quad [1 : M_T] \tag{A.2}$$

- The error is white:

$$E(e(k)e(k')) = \sigma_e^2 \delta(k - k') w^{-1}(k) \tag{A.3}$$

- The estimation, $\hat{\zeta}_e(k)$, is unbiased:

$$E(\tilde{\zeta}_e(k)) = 0 \tag{A.4}$$

- The covariance matrix of $\tilde{\zeta}_e(k)$ is denoted:

$$E(\tilde{\zeta}_e(k)\tilde{\zeta}_e(k')^T)) = Q^{\zeta_e}(k, k') \tag{A.5}$$

- Sensitivities respectively to θ^* and $\zeta_e(k)$ are defined as:

$$g_{\theta^*}(k, \theta^*, \zeta_e(k)) = \frac{\partial y(k, \theta^*, \zeta_e(k))}{\partial \theta^*} \tag{A.6}$$

$$g_{\zeta_e(k)}(k, \theta^*, \zeta_e(k)) = \frac{\partial y(k, \theta^*, \zeta_e(k))}{\partial \zeta_e(k)} \tag{A.7}$$

Note that the error $e(k)$ is defined in (A.1), with $y^{mes}(k)$, $k = 1, \ldots, M_T$, corresponding to measurements of elution peaks. Parameters $\zeta_e(k)$, $k = 1, \ldots, M_T$, correspond to the flow rate, the calibration coefficients and the injected concentrations and volume which are respectively imposed by the pump, determined by simple experiments, prepared by the user (see Section 3.4) and injected manually. Hence, the distribution of $e(k)$ and of $\zeta_e(k)$ are uncorrelated:

$$E(\tilde{\zeta}_e(k)e(k')^T)) = 0 \quad \forall \quad k, k' = 1, \ldots, M_T \tag{A.8}$$

The confidence interval on $\hat{\theta}^*$ is calculated through these steps:

1. Calculation of the expression of $\tilde{\theta}^*$ The estimation of $\tilde{\theta}^*$ is obtained from the optimality condition:

$$\left.\frac{\partial J(\theta^*, \hat{\zeta}_{e_v})}{\partial \theta^*}\right|_{\theta^* = \hat{\theta}^*} = -2\sum_{k=1}^{M_T} (y^{mes}(k) - y(k, \hat{\theta}^*, \hat{\zeta}_e(k))) g_{\theta^*} (k, \hat{\theta}^*, \hat{\zeta}_e(k)) w(k) = 0 \tag{A.9}$$

A Taylor series development of $y(k, \hat{\theta}^*, \hat{\zeta}_e(k))$ around $(k, \theta_{tr}^*, \zeta_{etr}(k))$, where high order terms may be neglected, is performed. Moreover, it is assumed that in the neighbourhood of $(\hat{\theta}^* \approx \theta_{tr}^*, \hat{\zeta}_e(k) \approx \zeta_{e_{tr}}(k))$,

$$g_{\theta^*}^T(k, \hat{\theta}^*, \hat{\zeta}_e(k)) \approx g_{\theta^*}^T(k, \theta_{tr}^*, \zeta_{e_{tr}}(k)) \quad \text{and}$$

$$g_{\zeta_e(k)}^T(k, \hat{\theta}^*, \hat{\zeta}_e(k)) \approx g_{\zeta_e(k)}^T(k, \theta_{tr}^*, \zeta_{e_{tr}}(k)) \tag{A.10}$$

The following expression is then obtained:

$$\tilde{\theta}^* \approx P_{M_T} \sum_{k=1}^{M_T} g_{\theta^*}(k, \theta_{tr}^*, \zeta_{e_{tr}}(k)) w(k) (e(k) - g_{\zeta_e(k)}^T(k, \theta_{tr}^*, \zeta_{e_{tr}}(k)) \tilde{\zeta}_e(k)) \tag{A.11}$$

2. Calculation of $(\tilde{\theta}^*\tilde{\theta}^{*T})$

This is performed by simple multiplication.

3. Calculation of the estimation of the expectation of $\tilde{\theta}^*\tilde{\theta}^{*T}$, $\hat{E}(\tilde{\theta}^*\tilde{\theta}^{*T})$

The following result is obtained using assumptions and definitions (A.1)–(A.8):

$$\hat{E}(\tilde{\theta}^*\tilde{\theta}^{*T}) = \hat{P}_{M_T}\sigma_e^2 + \hat{P}_{M_T}\left[\sum_{k'=1}^{M_T}\sum_{k=1}^{M_T} g_{\theta^*}(k,\hat{\theta}^*,\hat{\zeta}_e(k))w(k) \times g^T_{\zeta_e(k)}(k,\hat{\theta}^*,\hat{\zeta}_e(k))Q^{\zeta_e}(k,k') \quad g_{\zeta_e(k')}(k',\hat{\theta}^*,\hat{\zeta}_e(k')) \times w(k')g^T_{\theta}(k',\hat{\theta}^*,\hat{\zeta}_e(k'))\right]\hat{P}_{M_T} \tag{A.12}$$

4. Estimation of the covariance of $e(k)$, σ_e^2, to be used in the expression of $\hat{E}(\tilde{\theta}^*\tilde{\theta}^{*T})$

This estimation is obtained after 2 steps:

- the calculation of Taylor series development of the cost function $J(\theta^*, \zeta_{e_v})$ around $\theta^*_{tr} \approx \hat{\theta}^*$ and $\zeta_{e_{tr}}(k) \approx \hat{\zeta}_e(k)$, $\quad k = 1, \ldots, M_T$:

$$J(\theta^*_{tr}, \zeta_{e_{v_{tr}}}) \approx \sum_{k=1}^{M_T}\hat{e}^2(k)w(k) - \sum_{k=1}^{M_T}\left.\frac{\partial J(\theta^*,\zeta_{e_v})}{\partial\zeta_e(k)^T}\right|_{\hat{\theta}^*,\hat{\zeta}_e(k)}\tilde{\zeta}_e(k) + \sum_{k=1}^{M_T} g^T_{\theta^*}(k,\theta^*_{tr},\zeta_{e_{tr}}(k))\tilde{\theta}^*\tilde{\theta}^{*T}g_{\theta}(k,\theta^*_{tr},\zeta_{e_{tr}}(k))w(k) + \sum_{k=1}^{M_T}\sum_{k'=1}^{M_T}\sum_{k^*=1}^{M_T} g^T_{\zeta_e(k)}(k^*,\theta^*_{tr},\zeta_{e_{tr}}(k*))\tilde{\zeta}_e(k)\tilde{\zeta}_e(k')^T g_{\zeta_e(k')} (k^*,\theta^*_{tr},\zeta_{e_{tr}}(k^*))w(k^*) + 2\sum_{k=1}^{M_T}\sum_{k^*=1}^{M_T} g^T_{\zeta_e(k)}(k^*,\theta^*_{tr},\zeta_{e_{tr}}(k^*))\tilde{\zeta}_e(k)\tilde{\theta}^{*T}g_{\theta}(k^*,\theta^*_{tr},\zeta_{e_{tr}}(k^*))w(k^*) \tag{A.13}$$

- the calculation of the expectation of the preceding result:

$$M_T\sigma_e^2 = E\left(\sum_{k=1}^{M_T}\hat{e}^2(k)w(k)\right) - 2\sum_{k=1}^{M_T}\sum_{k^*=1}^{M_T} g^T_{\zeta_e(k^*)}(k^*,\theta^*_{tr},\zeta_{e_{tr}}(k^*)) \times Q^{\zeta_e}(k^*,k)g_{\zeta_e(k)}(k^*,\theta^*_{tr},\zeta_{e_{tr}}(k^*))w(k^*) + \sum_{k=1}^{M_T} g^T_{\theta^*}(k,\theta^*_{tr},\zeta_{e_{tr}}(k))E(\tilde{\theta}^*\tilde{\theta}^{*T})g_{\theta^*}(k,\theta^*_{tr},\zeta_{e_{tr}}(k))w(k) + \sum_{k=1}^{M_T}\sum_{k'=1}^{M_T}\sum_{k^*=1}^{M_T} g^T_{\zeta_e(k)}(k^*,\theta^*_{tr},\zeta_{e_{tr}}(k*)) \times Q^{\zeta_e}(k,k')g_{\zeta_e(k')}(k^*,\theta^*_{tr},\zeta_{e_{tr}}(k^*))w(k^*) \tag{A.14}$$

5. Introduction of the covariance of $e(k)$, Eq. (A.14), in $\hat{E}(\tilde{\theta}^*\tilde{\theta}^{*T})$ (Eq. (A.12))

Appendix B.

Model parameters.

Table A.1
Calibration factors of the UV detectors.

	UVA	UVB
Detector UV1	0.227	0.219
Detector UV2	0.206	0.199
Detector UV3	0.1991	0.1919
Detector UV4	0.215	0.207

Table A.2
Moving dead volume.

Position (at start-up)	$V_{D,p}^{col,b}$ (m^3)	$V_{D,p}^{col,af}$ (m^3)
1	1.88e−6	1.07e−6
2	1.88e−6	3.07e−6
3	0.95e−6	0.145e−6
4	1.88e−6	1.07e−6
5	1.88e−6	1.07e−6
6	0.95e−6	0.145e−6
7	1.88e−6	1.07e−6
8	1.88e−6	3.07e−6
9	0.95e−6	0.145e−6
10	1.88e−6	1.07e−6
11	1.88e−6	1.07e−6
12	0.95e−6	0.145e−6

Table A.3
Fixed dead volume.

Position (at start-up)	$V_{D,p}^{port,b}$ (m^3)	$V_{D,p}^{port,af}$ (m^3)
1	0.655e−6	0.925e−6
2	0.195e−6	0.925e−6
3	0.195e−6	2.235e−6
4	5.35e−6	0.925e−6
5	0.195e−6	0.925e−6
6	0.195e−6	0.605e−6
7	0.655e−6	0.925e−6
8	0.195e−6	0.925e−6
9	0.195e−6	2.695e−6
10	5.595e−6	0.925e−6
11	0.195e−6	0.925e−6
12	0.195e−6	0.605e−6

References

[1] D.M. Ruthven, C.B. Ching, Chem. Eng. Sci. 44 (5) (1989) 1011.
[2] J. Strube, U. Altenhöner, M. Meurer, H. Schmidt-Traub, M. Schulte, J. Chromatogr. A 769 (1997) 81.
[3] J. Strube, H. Schmidt-Traub, Comput. Chem. Eng. 22 (9) (1998) 1309.
[4] L.S. Pais, J.M. Loureiro, A.E. Rodrigues, Chem. Eng. Sci. 52 (2) (1997) 245.
[5] S. Lehoucq, D. Verhève, A. Vande Wouwer, E. Cavoy, S.M.B. Enantioseparation, AIChE J. 46 (2000) 2.
[6] J. Haag, A. Vande Wouwer, S. Lehoucq, P. Saucez, Control. Eng. Pract. 9 (2001) 921.
[7] Y.A. Beste, M. Lisso, G. Wozny, W. Arlt, J. Chromatogr. A 86 (2000) 169.
[8] D. Antos, A. Seidel-Morgenstern, Chem. Eng. Sci. 56 (2001) 6667.
[9] C. Migliorini, M. Mazzoti, M. Morbidelli, AIChE J. 45 (1999) 7.
[10] M. Pedeferri, G. Zenoni, M. Mazzotti, M. Morbidelli, Chem. Eng. Sci. 54 (1999) 3735.
[11] S. Abel, G. Erdem, M. Mazzoti, M. Morari, M. Morbidelli, J. Chromatogr. A 1092 (2005) 1.
[12] S. Katsuo, C. Langel, P. Schanen, M. Mazzotti, J. Chromatogr. A 1216 (2009) 1084.
[13] V. Grosfils, C. Levrie, M. Kinnaert, A. Vande Wouwer, Chem. Eng. Sci. 62 (2007) 3894.
[14] Knauer, CSEP C9 Series, Simulated Moving Bed Chromatography Systems, V0499, 2000.
[15] U. Altenhöner, M. Meurer, J. Strube, H. Schmidt-Traub, J. Chromatogr. A 769 (1997) 59.

[16] V. Grosfils, Ph.D. thesis, Modelling and parametric estimation of simulated moving bed chromatographic processes (SMB) Service d'automatique et d'analyse des sytèmes, ULB, 2009.
[17] A. Seidel-Morgentsern, J. Chromatogr. A 1037 (2004) 255.
[18] W.E. Schiesser, Integration of Partial Differential Equations, Academic Press, San Diego, CA, 1991.
[19] J. Haag, Dynamic modelling and state estimation of complex bioprocesses-theoretical issues and applications, PhD thesis, FPMs, 2003.
[20] M.J.D. Powell, UOBYQA: unconstrained optimization by quadratic approximation, Report DAMTP 2000/NA14, 2000.
[21] V. Grosfils, Technical report, Estimation of an upper bound of the error on the initial estimated, ULB, 2007.
[22] G.A.F. Seber, C.J. Wild, Nonlinear Regression, John Wiley & Sons, New York, 1989.
[23] G. Guiochon, J. Chromatogr. A 965 (2002) 129.